Journal of Applied Polymer Science

Embedded macroporous elastomers by hydrostatic fracturing for flexible strain-sensor applications

Kumar Phanishwar, Shama Perween, Neelam Saurakhiya, Amit Ranjan
Department of Chemical Engineering, Rajiv Gandhi Institute of Petroleum Technology, Ratapur Chowk, Raebareli, Uttar Pradesh 229010, India
Correspondence to: A. Ranjan (E-mail: aranjan@rgipt.ac.in)

ABSTRACT: A method is proposed for fabricating flexible materials embedded with macroporous regions by inducing fractures under point loading. Possible use of these structures in strain sensing is demonstrated. Injecting air at high pressure through a needle-tip generates 3-dimensional fractures in homogeneously crosslinked polydimethylsiloxane (PDMS) media, whereas a 2-dimensional planar fracture is generated in a sandwich-like structure wherein a softer layer is bounded by two stiffer layers. Size-dependence of 3-dimensional fractures on stiffness of the media which is controlled by the crosslinker concentration shows a maximum, suggesting an optimal stiffness for generating largest fracture. The size of the 2-dimensional fractures (~5 cm) generated inside the sandwiched layer is huge as compared to the 3-dimensional fractures (~1 mm) under the similar conditions. Two dimensional fractured surfaces show ridges with feature length monotonically becoming smaller with stiffness. Embedded rough planar domains are created by introducing 2-dimensional fractures at distances close enough to overlap. Using this method an embedded 2-dimensional porous domain of polyaniline nanostructures is realized in flexible PDMS matrix. An Ohmic nature of these embedded polyaniline domains with an ability to change resistance under compression establishes their suitability for developing inexpensive and flexible strain sensors.
 J. Appl. Polym. Sci. **2016**, *133*, 43681.

KEYWORDS: conducting polymers; inorganic polymers; sensors and actuators

Received 18 October 2015; accepted 23 March 2016
DOI: 10.1002/app.43681

INTRODUCTION

Fracture and crack propagation in "hard" inorganic materials such as metals and ceramics have been widely studied.[1–5] However, fracture in soft and viscoelastic polymeric materials is relatively less understood.[6–8] Most of the studies have focused on adhesive fracturing[9–12] and some on cohesive fracturing.[13,14] However the cohesive fractures studied in terms of crazing and failure in glassy polymers[15–22] and network-gels and elastomers,[13,23,24] both theoretically and experimentally, are concerned with failure of the material under opening mode (tearing) also known as mode I loading geometry. In this article, we examine fractures generated by hydrostatic pressure caused by localized point loading. Fracture behavior is very sensitive to structural disorder and the mechanical properties of the matrix. It is particularly challenging to understand fractures in viscoelastic polymeric materials owing to the presence of long chain molecules which impart a significant entropic contribution to the equilibrium thermodynamic properties of the material. Furthermore, because of the complex interactions present between the long chain-like molecules, their deformation and flow properties also assume complexity. On application of stress, the failure-generated crack in an otherwise homogeneous polymer-based viscoelastic material can result either from bond-breakage or from complete separation of two entangled chain molecules. The former has a solid-like character leading to irreversible generation of damage, whereas the latter has liquid-like nature, which can disappear with time due to polymer relaxation under flow. Relative importance of these two effects plays the governing role in determining the size and morphology of the fracture-generated surfaces in viscoelastic materials. In an earlier study, similar aspects were investigated[25] in surfaces generated by tearing or enforcing cohesive failure in viscoelastic elastomers. In Ref. 25, we studied cohesive failure under plane stress conditions generated by distributed extensional loading. In this article, we adopt a complementary approach and study fractures in soft viscoelastic elastomers formed under point loading that generates three-dimensional hydrostatic pressure. The process is somewhat similar to that of hydraulic fracturing, a frequently practiced technique in oil and gas industry. In hydraulic fracturing, a recently developed process for extraction of shale gas from the rock pores, a fluid is injected at a pressure larger or commensurate with the compression modulus of the formation

through the drill hole which leads to fracturing of the rocks and thereby releasing the trapped gases. Here we use similar technique of inducing fractures in soft viscoelastic materials. In a related study, Das and Ghatak[26] investigated the stick–slip behavior in force–displacement curve while gels are ruptured by the point-loading due to the tip of a moving needle. However, the fracture in their case was generated by shear and not by hydrostatic pressure. Our current work has both fundamental and practical aspects to it. Correlation of the size of the fracture with the stiffness of the medium and injection pressure is established based on the basic polymer physics ideas. Practical applicability of our method which we demonstrate in this paper lies in utilizing these fractures to fabricate flexible macroporous material which can find potential use in strain sensing and gas sensing. For example, in this article we have realized an embedded polyaniline porous domain showing Ohmic behavior and exhibiting change in resistance with an applied mechanical compression in the parent matrix. Organization of this paper is as follows: In the Section "Experimental", we present the methodology of generating the fracture and dependence of the fracture size on the material properties and load. In Section "Results and Discussion" we present the result of localized swelling used for shrinking the size of the fracture. This is followed by fabrication of macroporous domains comprising of overlapping fractures in Section "Results and Discussion." Here we also discuss an application of these macroporous domains by synthesizing nanostructured polyaniline embedded in the polydimethylsiloxane (PDMS) demonstrating the possibility of fabrication of such embedded macroporous nanostructures via this method. We conclude in Section "Conclusions" with a discussion on scope and future work.

EXPERIMENTAL

We have used Sylgard-184 from Dow Corning, Midland, MI, USA as our working elastomeric material. This contains both the pre-polymer and the crosslinker. The network of PDMS formed of Sylgard-184 is studied at different degrees of crosslinking. The PDMS was thoroughly mixed with the crosslinker, degassed to remove trapped air bubbles, and cured. THF was used as a solvent to swell the crosslinked PDMS. Optical microscopy was performed using Leica microscope. Aniline (99% purity) and potassium dichromate (99.5% purity) from Qualigens, Mumbai, India were used. Sulfuric acid (98% purity) from Merck, Mumbai, India was used. The chemical were used as received without any further purification. A home-made setup schematically shown in Figure 1(a) was utilized for generating embedded fractures.

Synthesis of conducting polymer polyaniline into the fracture has been completed in following manner. The three stock solutions were prepared in order to achieve resultant polyaniline (PANI) structures. First, a solution (S1) 0.3 *M* aniline monomer in DI water (Milli-Q ~18 M Ω cm) was prepared by mixing rigorously for few minutes to make a homogenous solution. The second solution (S2) of 3 *M* H_2SO_4 in DI water was also prepared and then the third solution (S3) was prepared by mixing 0.294 g of $K_2Cr_2O_7$ in 10 mL of DI water in the presence of two-three drops of S2. About 5 mL of S1 was then mixed with 0.5 mL of S2 in order to make a fourth solution (S4) of

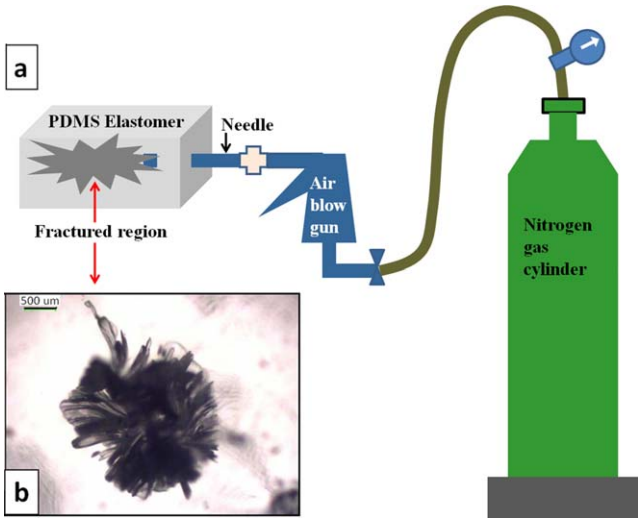

Figure 1. (a) The schematic diagram of the set up used for creating fractures (not drawn to scale). (b) An optical micrograph image of a 3D fracture created in a sample block of elastomer with 2.2 weight percent crosslinker sample. [Color figure can be viewed in the online issue, which is available at wileyonlinelibrary.com.]

$1 < pH < 2$ and this solution was taken in a syringe. Similarly, 0.5 mL of S3 was taken into another syringe. The needles from these two syringes were placed oppositely so as to inject these chemical in the fracture. After injecting the two solutions, the PANI structures were synthesized immediately after injecting the solutions within the closed confinement of the fracture. The color of the deposited structure was algae-green.

Optical images were acquired using Leica optical microscope (model DM750P). Scanning electron microscopy (SEM) images were acquired using Zeiss machine (model Supra-40VP). For measuring the IV characteristic, Aplab regulated DC power supply (model LQ6324) was used to generate constant current and the Aplab VC97 multimeter was used for voltage measurements. Controlled compression was achieved by using compression grip in a Tinius Olsen Universal Testing Machine (model H25KS).

The Perkin Elmer Spectrum Two FTIR spectrometer was used to record the FTIR spectra of the samples as either solid or thin film. All the samples were recorded using "attenuated total reflectance" (ATR) mode. The PIKE MIRacle single reflection horizontal ATR accessory equipped with a ZnSe ATR crystal was used for recording the FTIR spectra. The polymer samples of the small molecules were pressed against the ATR crystal to record the spectra. The spectra were collected at 4 cm^{-1} spectral resolution utilizing a 1 min data collection time.

The needle attached to the air-blow gun was injected inside the polymer samples and nitrogen was discharged at a fixed applied pressure. The formation of the fracture was almost immediate. The trigger time was manually controlled and kept same for all the samples.

RESULTS AND DISCUSSION

Two-Dimensional and Three-Dimensional Fractures

We have been able to generate 3D as well as 2D fractures in PDMS samples. In a material with uniform crosslinker

concentration (ranging from 2 to 4%) ensured by thorough mixing and degassing, our procedure yields 3D fractures. However, in sample blocks having a sandwich structure wherein the region with low-crosslinker density lies between those with high crosslinker density (10%) resulting into a soft region surrounded between two stiff boundaries, the same procedure yields planar fractures with planes oriented parallel to the stiff boundaries. Also, the size of these planar fractures measured in terms of their planar spans is very large as compared to the 3D fractures generated under same conditions. Here, we first study the overall size of a 3D fracture which shows a non-monotonic dependence on the crosslinker concentration (and hence the stiffness of the sample), and then present the surface morphology of the planar (2D) fractures showing a monotonic trend in their feature length with the crosslinker concentration. Figure 1(b) shows a typical 3D fracture generated. We emphasize here that this article will examine only the overall size of 3D fractures, whereas for the 2D fractures, we will also look at the surface morphology in detail using optical and electron microscopy as the latter is used in the fabrication of sensor elements.

We studied the size of the 3D fractures as functions of the applied pressure and crosslinker density. The crosslinker density was varied from 2.2 to 3%. This particular range was chosen as this variation in crosslinker density concentration leads to significant change in the elastic modulus of the crosslinked PDMS. In samples with crosslinker densities exceeding 3%, the fractures did not form at all. Figure 2 shows that the dependence of the mean size of the fracture with crosslinking at different pressures is non-monotonic. Interestingly a non-monotonic trend is observed: The mean size increased at low crosslinking and decreased at high crosslinking. We considered the crosslinking of up to 2.7% because at higher crosslinking the material becomes too stiff to be fractured and the air-leakage is unavoidable causing a large noise in the data.

The counterintuitive dependence of the fracture size on crosslinking can be explained by employing the idea of strain-rate dependent surface tension arising in viscoelastic materials as proposed by Persson and Brener.[27] Persson and Brener suggested that when a crack propagates in a viscoelastic material, an effective surface tension is to be considered to account for the energetics which originates from the dissipative losses occurring in the regions lying nearby the deforming surfaces. They derived an expression for the effective surface tension γ and is found to vary with v_c, the crack propagation speed, as following:

$$\gamma \sim (v_c)^{1/3} \tag{1}$$

In our problem v_c can be identified as the temporal rate of change of the size of the fracture. An estimate of the size of the fracture can be made by considering the energetics of the process. If the size of a fracture changes from r to $r + dr$ then an additional surface energy of $\gamma \Delta A = 8\pi\gamma r dr$ is spent at the cost of the elastic energy $G' dV = 4G'\pi r^2 dr$ released by the volume. Here G' is the storage modulus of the PDMS network material. The fracture size is obtained by equating the surface and bulk energy which yields:

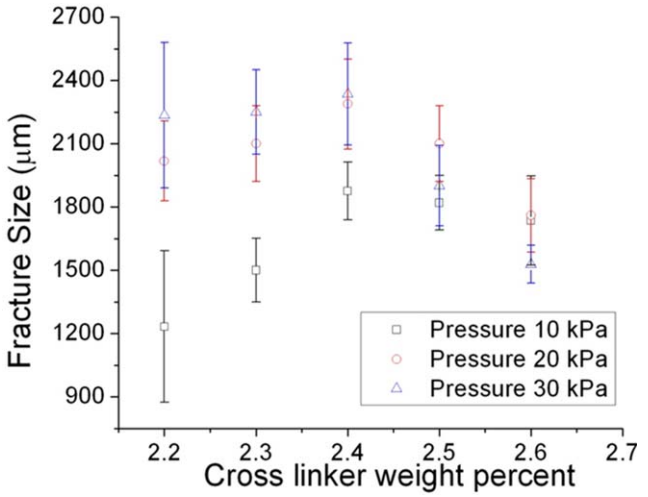

Figure 2. Dependence of fracture size on weight percent of crosslinking agent. [Color figure can be viewed in the online issue, which is available at wileyonlinelibrary.com.]

$$r \approx 2\gamma/G' \sim (v_c)^{1/3}/G'. \tag{2}$$

As the degree of crosslinking is increased, the storage modulus G' increases and v_c at a given discharge pressure decreases (because of increased stiffness), which explains the reduction in size of the fracture with degree of crosslinking at higher crosslinking percentage. However, at low crosslinking, the PDMS network is an imperfect network possessing a significant fraction of dangling chain ends. For such imperfect networks, G' is known to depend on the characteristic frequency ω as $G' \sim \omega^{1/2}$.[28] This dependence arises due to Rouse-like dynamics of the relaxing strands in the network. It is to be noted that this dependence is more effective at low crosslinking since G' tends to become constant with frequency at high crosslinking density. The deformation frequency can be approximated by $\omega \sim v_c/r$, which gives $G' \sim (v_c/r)^{1/2}$ for Rouse-like relaxation dynamics for the imperfect network. Substituting this for G' in eq. (2), we get $r \sim (v_c)^{-1/3}$. Since v_c decreases with crosslinking (as material becomes stiffer), based on our foregoing considerations, we conclude that the size of the fracture will increase at low crosslinking density. Thus the non-monotonicity in the fracture size dependence on crosslinking can be explained by utilizing Persson's theory of effective surface tension. A physical picture may be presented as follows: At low crosslinking, the material is less stiff allowing faster deformation. But for faster deformation, viscous dissipation due to the relaxing strands of polymers is high and therefore energy expenditure is larger for the same volume change. This results into smaller size at low crosslinking. The viscous losses also govern sensitivity of the fracture-size to applied pressure which can be seen to decrease at higher crosslinking.

We next present our results on 2D fractures generated in sandwiched structures. The sandwiched structures were amenable to generation of 2D fractures up to a larger concentration of the crosslinker (~4%) unlike the 3D structures which failed to form beyond a crosslinking density of 2.6%. We have examined the surface morphology of the 2D fractures at two different

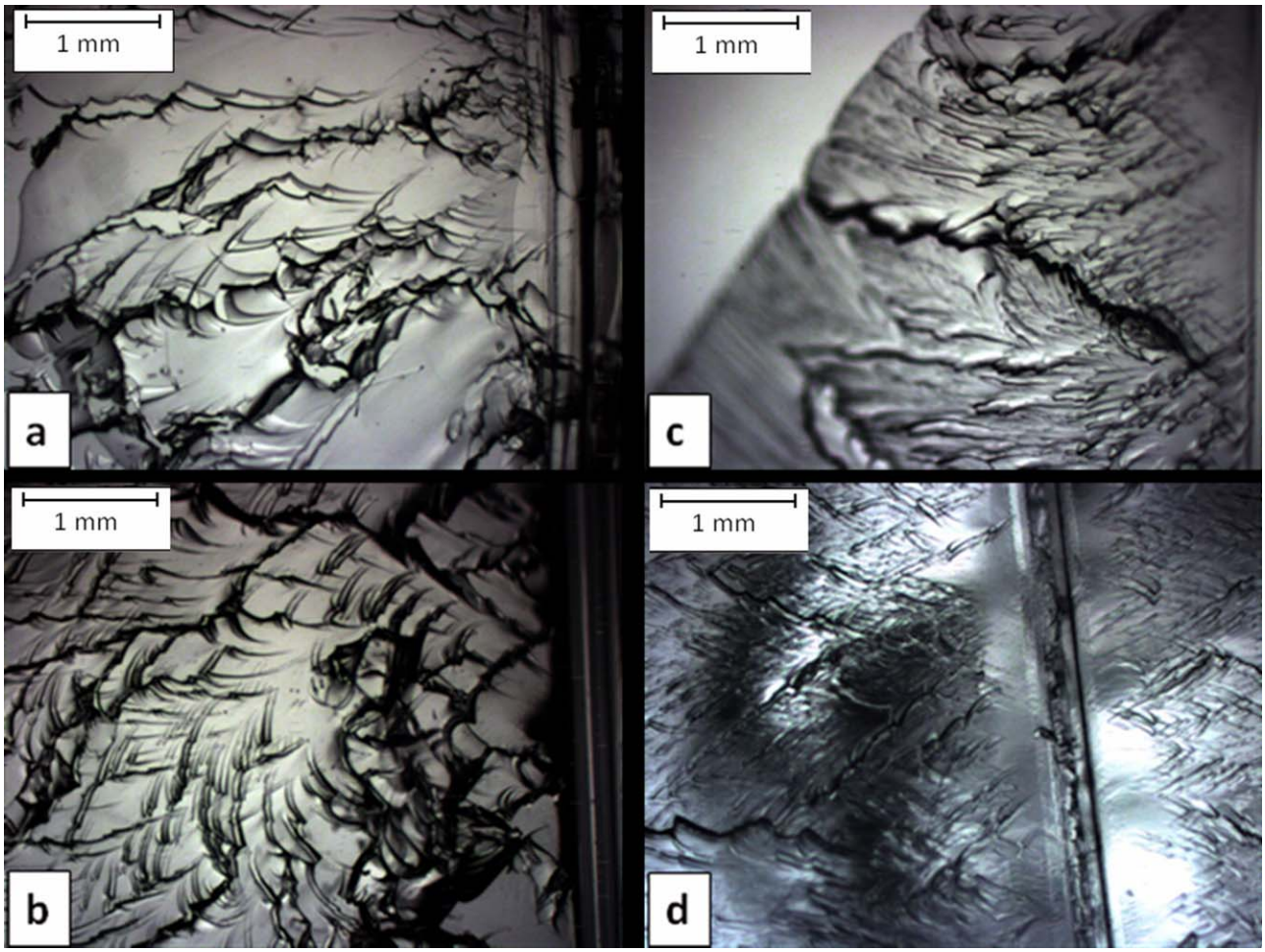

Figure 3. The optical micrographs of the planar fractures created in samples with crosslinker weight percents of (a) 2.2, (b) 2.6, (c) 3.2, and (d) 3.6. [Color figure can be viewed in the online issue, which is available at wileyonlinelibrary.com.]

length scales by imaging these surfaces using optical microscopy as well as SEM. On both scales, the features show ridges whose spacing decreases with the crosslinking concentration. Figure 3 shows the optical micrograph of the surface morphology of the 2D surfaces generated due to fractures in samples with increasing crosslinking concentration with a fixed pressure. It is evident that higher crosslinked material presents a more ridged surface whereas at lower crosslinking the surface becomes smoother. This result suggests that crosslinking can be used as a means to control the exposed surface area which is important if we aim to functionalize these surfaces. It is also an important parameter governing the porosity and permeability of the macroporous region formed when multiple fractures overlap. Figure 4 shows the SEM images of the 2D fractured surfaces at various crosslinking concentrations. A similar trend as observed in optical micrographs, that is, the spacing between ridges becoming smaller with increase in stiffness, is observed in these images also. Thus, in addition, it can also be observed that the ridges run more or less parallel without any interconnections in low crosslinked systems, whereas at higher crosslinking, the interconnecting features become more frequent. This effect can be attributed to the fact that at low cross-linking the fluid-like deformation is dominant which imparts directionality to these features. At larger crosslinker density, solid-like bond breakage leads to wrinkling features in a direction perpendicular to the parallel ridges.

Shrinkage of 2-Dimensional Fractures by Localized Swelling

Swelling, patterning, and subsequent de-swelling has been employed for miniaturization of feature size in elastomers.[29] This technique relies on inducing global swelling in the material by immersing the network material in the solvent. Since the entire material swells in size, any feature generated in the swollen material will be shrunk after the material loses solvent on de-swelling. This method was used to miniaturize the surface features on an elastomeric material.

Here, we adopt a somewhat complementary approach of localized swelling which leads to reduction in fracture size. The step involves injecting the solvent (THF) in the elastomer (PDMS) inside the fracture. This single post-generation processing step leads to shrinkage of the fractures as explained in Figure 5(a,b). Due to localized swelling the inner surface of the fracture swells inward as the region far away from the fracture cannot experience any expansion due to swelling. A fracture undergoing size reduction on localized swelling is shown in Figure 5(c,d). This method offers a simple route to size reduction of the fracture.

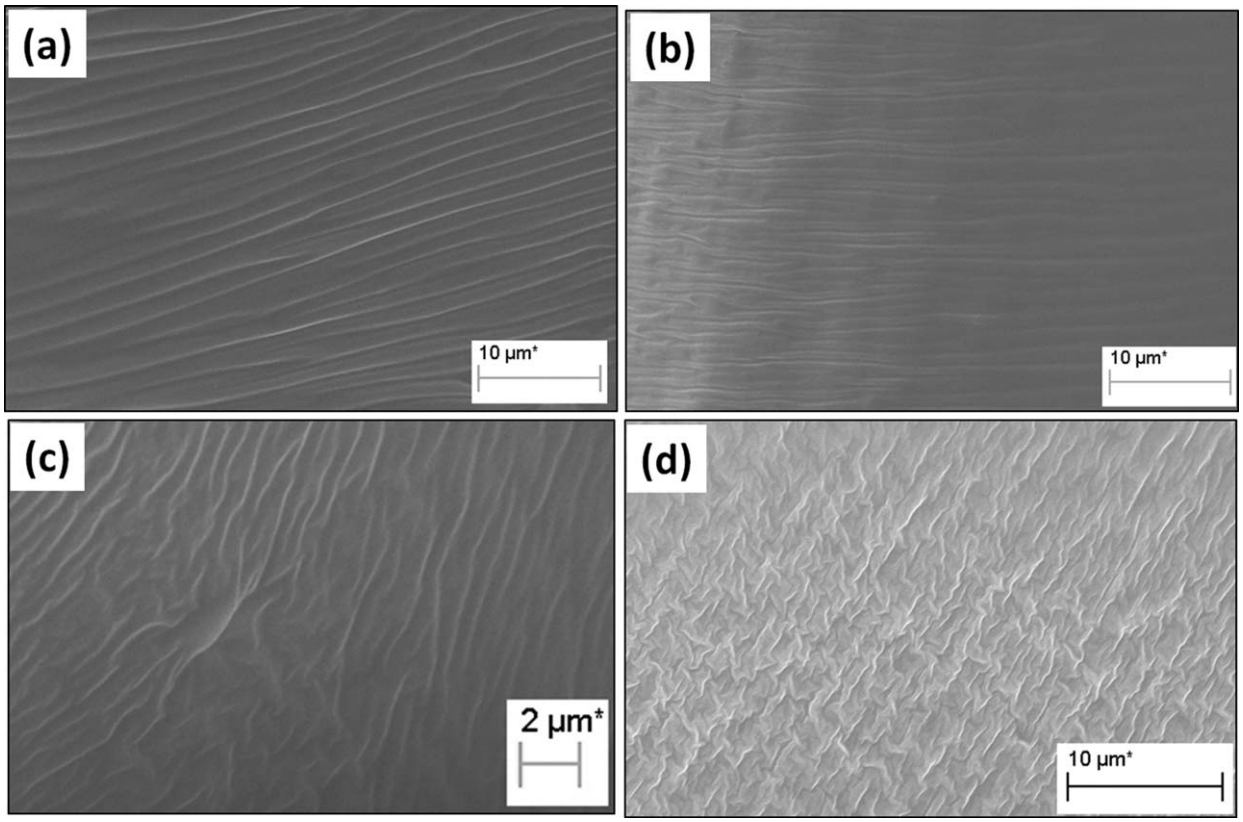

Figure 4. SEM images of the planar fractures created in samples with crosslinker weight percents of (a) 2.2, (b) 2.6, (c) 3.2, and (d) 3.6.

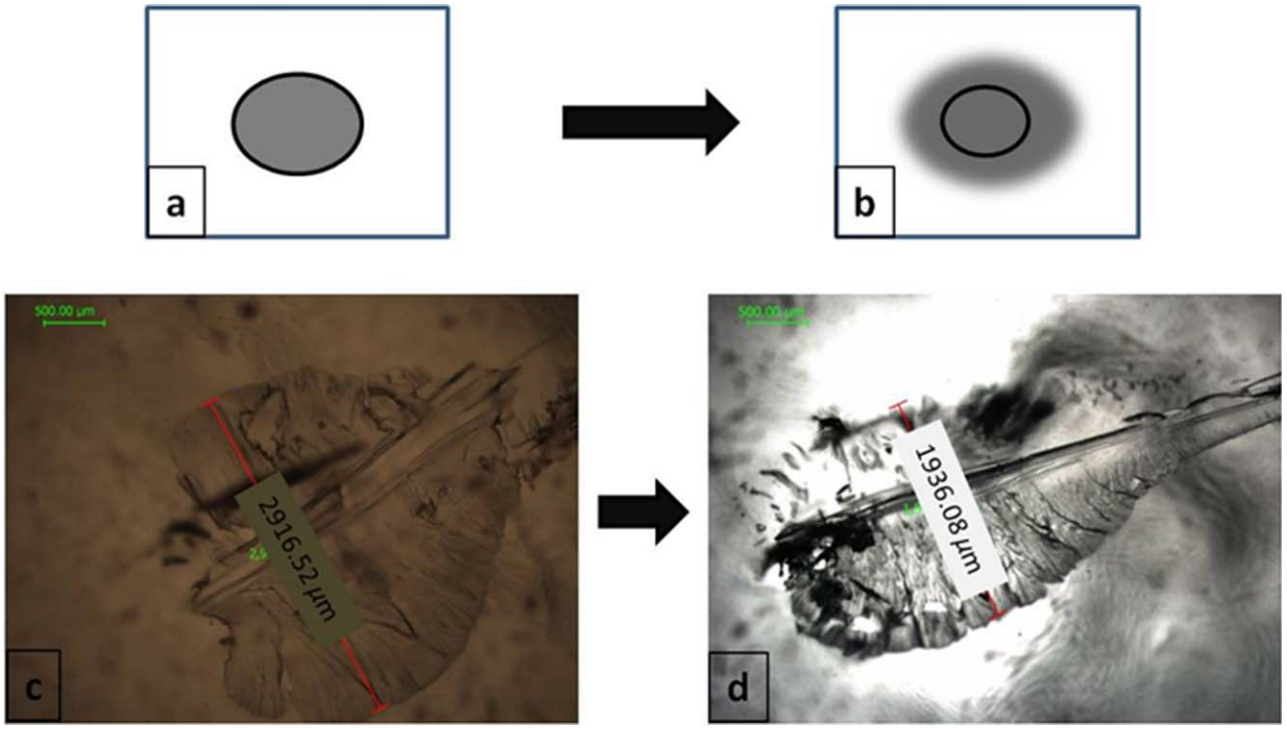

Figure 5. (a) and (b) show the schematic of how localized swelling leads to contraction of an embedded crack. The shaded portions in (a) and (b) represent the solvent fluid which swells the medium. The elliptical dark line represents the inner boundary of the crack that contracts after swelling. (c) and (d) show the optical micrographs of a crack respectively before and after injecting THF solvent which swells PDMS. [Color figure can be viewed in the online issue, which is available at wileyonlinelibrary.com.]

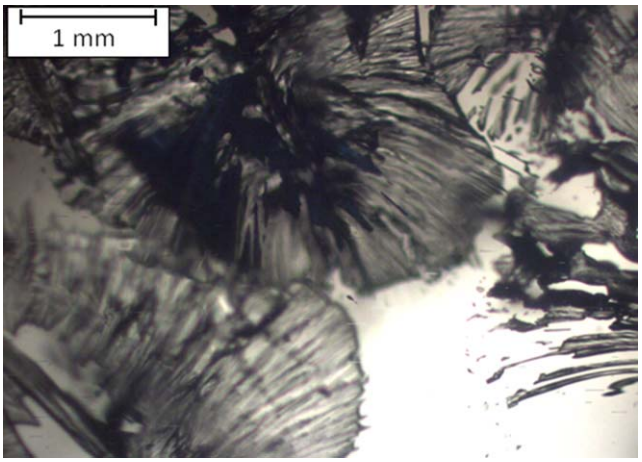

Figure 6. Optical micrograph of multiple overlapping planar fractures. Scale bar is 1 mm. [Color figure can be viewed in the online issue, which is available at wileyonlinelibrary.com.]

Furthermore, we believe that this technique can be fruitfully used to line the fracture surfaces with nanoparticles (and thereby functionalize them) by injecting the cavity with a suitable nanoparticle suspension.[31,32] Under the effect of osmotic forces, the solvent will carry the nanoparticles to the subsurface region.

Embedded Macroporous Domains via Multiple Overlapping Fractures as a Compression Sensor Element

Next we turn our attention to (i) formation of macroporous domains generated by introducing multiple overlapping fractures, and (ii) generation of polyaniline nanostructures in these macroporous domains. Macroporous materials may find use in various applications such as membranes, micro-reactors, microfluidics, and gas storage to name a few. Our method of introducing fractures of controlled size and surface morphology enables us to fabricate embedded macroporous domains in elastomeric materials by introducing fractures which overlap in its spatial extent.

Figure 6 shows an optical micrograph of several fractures overlapping in their spatial extent. Overlap of the fractures establishes connectivity between different portions of the elastomer through a macroporous domain. The surface area of the macroporous domain is dependent on the load and degree of crosslinking as discussed earlier. Porosity and permeability of these macroporous regions generated under different conditions will be analyzed in detail elsewhere along with the analysis of the morphology of the fracture generated surfaces.

We next synthesize polyaniline nanoparticles inside these microporous domains. Polyaniline nanostructures are promising materials in sensors, chemical catalysis, reactive membranes, and optoelectronics applications.[30] However, these polymers lack mechanical integrity. If nanostructured polyaniline can be used in conjunction with a non-reactive, mechanically robust, and transparent material such as crosslinked PDMS, versatile technological components can be designed. To this end, we fabricate embedded nanostructured polyaniline domains inside a PDMS solid using our method. We were able to successfully fabricate a macroporous region in PDMS filled with nanostructured polyaniline by introducing the reactants through two opposite ends of a macroporous domain. Following standard protocol for synthesizing polyaniline using solution method,[31] aniline solution in sulfuric acid and the potassium dichromate solution were injected inside the macroporous domain from two widely separated ends using a syringe. The liquid phase reactants quickly spread over the macroporous volume and reacted to yield the product. The macroporous region turns algae-green in color after some time once the reaction is over, suggesting formation of polyaniline.

Figure 7 shows the FTIR spectra of the cured PDMS, polyaniline synthesized outside, and polyaniline synthesized inside the fractures. As seen from these spectra, a band around 1500 cm^{-1}, which is present in samples of polyaniline synthesized outside the fractures as well as those synthesized inside the fractures, is found absent in pure and cured PDMS samples. This confirms the presence of polyaniline in the fractured regions. Figure 8 shows the resulting polyaniline domain embedded inside the PDMS.

The polyaniline was also synthesized by the same method on a glass slide for comparison. The SEM images of the microporous polyaniline domains and those on the glass slide are presented for comparison in Figure 8(c,d). Difference in morphology in the two cases is evident. This may be attributed to the growth of polyaniline in a constrained geometry. The effect of chemical nature of the substrate can be ruled out because of the inertness of the PDMS.

These results suggest that our method can be used to prepare a medium where the influence of confinement on a chemical reaction can be studied in detail.

The porous embedded domains formed in 2D fractures were tested for their electrical conductivity. The blocks were

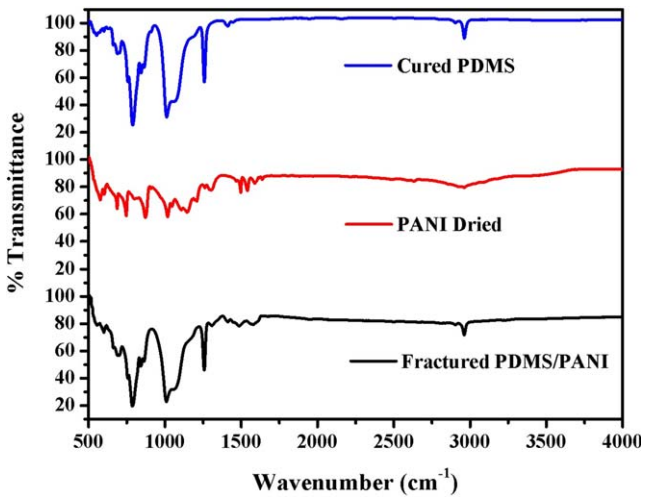

Figure 7. FTIR spectra of cured PDMS, polyaniline synthesized outside the fractures, and polyaniline synthesized inside the fractures. The presence of a band around 1500 cm^{-1} confirms the presence of polyaniline inside the fractured region. [Color figure can be viewed in the online issue, which is available at wileyonlinelibrary.com.]

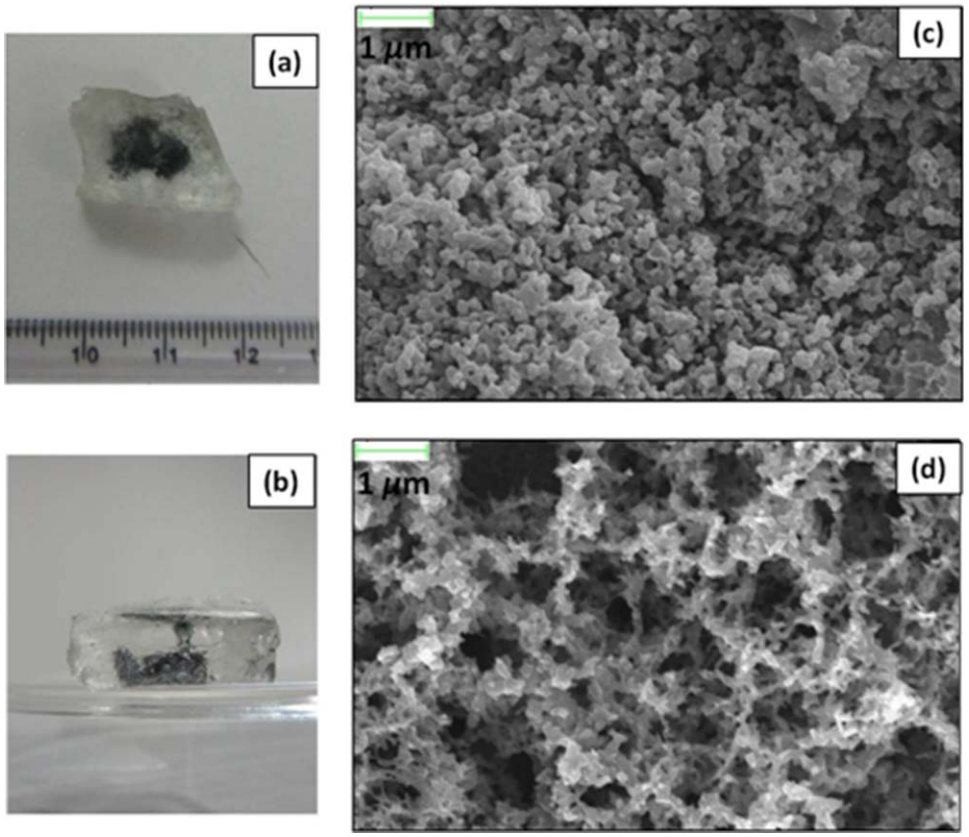

Figure 8. (a) and (b) show the top and side views of a microporous polyaniline domain embedded in PDMS. (c) SEM image of the embedded microporous domain of polyaniline. (d) SEM image of polyaniline synthesized by the same method but on a glass slide. The scale bars in (c) and (d) are 1 μm each. [Color figure can be viewed in the online issue, which is available at wileyonlinelibrary.com.]

compressed to different extents and the current voltage characteristic was measured at various values of compressions. The polyaniline domains showed ohmic behavior, with the resistance (measured by the slope of the best linear fit of the current vs. voltage data) a function of compression. The data is presented in the Figure 9 showing a gradual decrease in resistance with increasing compression. The resistance sensitivity is on the order of 5 k-Ω/μ of compression. This result suggests that we can design these macroporous polyaniline embedded PDMS blocks as flexible compression sensing elements. The detection limit in this work is around 80 microns, the smallest compression for which resistance change was measured.

Next, we propose a simple model and obtain an equation between resistance and compression that fits the data satisfactorily. In our model, we assume that the fractured surfaces consist of long protrusions of cylindrical geometry with constant cross-sectional area, coated with polyaniline nanostructures. Length of

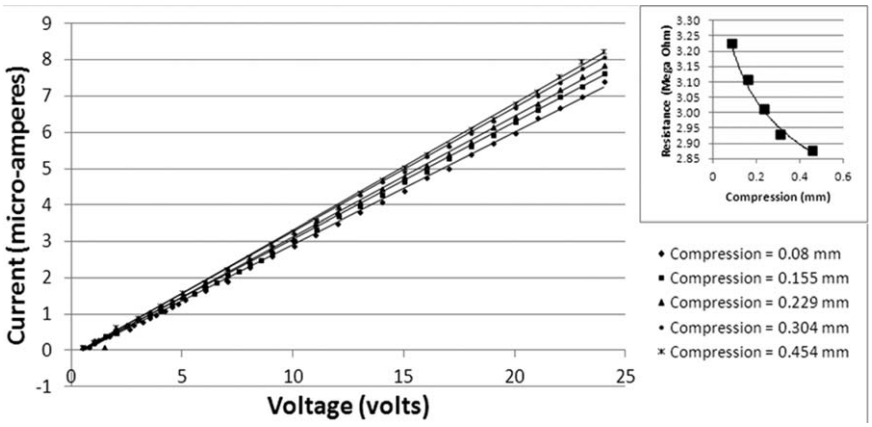

Figure 9. Current–voltage characteristics of the polyaniline embedded in PDMS 2-D fractures at different compressions. Inset shows the dependence of resistance with the compression. The solid lines in the main figure are linear fits and in the inset, a guide to the eye.

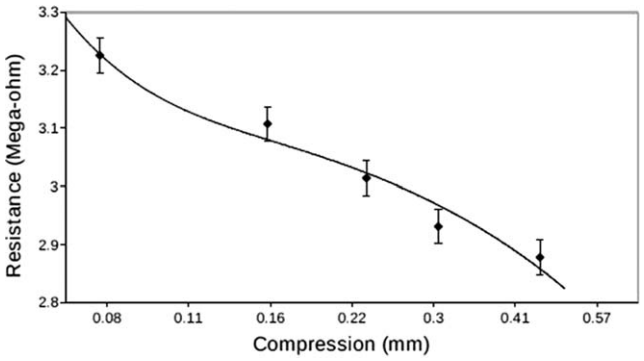

Figure 10. The fitting of the resistance-compression data to eq. (3) predicted from the proposed model.

the protrusions (x) is assumed to follow an exponential distribution with probability density given by $g(x) = (B/N)\exp(-xB/N)$, where N is the total number of the cylindrical protrusions, and B is a normalization constant with a dimension of inverse of length. As the block is compressed, the polyaniline nanoparticulate matter adhered to the polymeric cylindrical protrusions extending from either of the fractured surfaces get in contact. More and more cylindrical protrusions of increasingly smaller sizes come into contact that results into increase in the contact area with compression and a corresponding decrease in resistance. The increase in contact area, A, with compression, y, depends on the number distribution of the polymeric protrusions. Using the formula of resistance $R = \rho l/A$, where ρ is the resistivity of polyaniline material, l is the distance between two fractured planar surfaces and is given by $l = h - y$, where h is the initial separation, we get the following expression for dependence of R on y:

$$R(x) = \frac{M(h-y)}{1-\exp\left(\frac{-By}{N}\right)} \quad (3)$$

A plot of resistance vs. compression is presented in Figure 10. The solid line is a plot of the function with the following values of the fitting parameters: $M = 0.746$, $h = 4.277$, and $B/N = 43.78$. As evident from the plot, the experimental data satisfactorily fit the model proposed.

CONCLUSIONS

In summary, we have presented a study on generation of fracture in soft elastomers due to hydrostatic pressure applied locally. Two different geometries were realized to generate 3D and 2D fractures. The size of the 3D fracture depends on the degree of crosslinking, exhibiting an optimum crosslinking at a given pressure at which the size is maximum. The sensitivity to pressure is increasingly small as crosslinker density is increased. The feature size in 2D fractures generated in sandwiched geometry decreased with increasing crosslinking density. A flexible material with embedded macroporous region was fabricated by allowing spatial overlaps of these fractures. By incorporating conducting polyaniline in these embedded domains, an arrangement suitable for compression sensing applications was realized.

ACKNOWLEDGMENTS

This work was supported by the Department of Science and Technology, Government of India, Grant SB/S3/CE/016/2013. Authors thank Dr. Sandip Patil for helping with the design of the set-up and Mr. Rudra Kumar from Indian Institute of Technology Kanpur, India for helping with the SEM analysis of our samples

REFERENCES

1. Dieter, G. E. Mechanical Metallurgy; McGraw-Hill: London, **1988**.
2. Wilsdrof, H. G. F. *Mater. Sci. Eng.* **1983**, *59*, 1.
3. Thomason, P. F. *Acta Mater.* **1999**, *47*, 3633.
4. Pugh, S. F. *Br. J. Appl. Phys.* **1967**, *18*, 129.
5. Ravi-Chandar, K.; Yang, B. *J. Mech. Phys. Solids* **1997**, *45*, 535.
6. Gent, A. N.; Pulford, C. T. R. *J. Mater. Sci.* **1984**, *19*, 3612.
7. Cam, J.-B. L.; Toussaint, E. *Macromolecules* **2010**, *43*, 4708.
8. Mathew, A. *Eur. Polym. J.* **2001**, *37*, 1921.
9. Crosby, A. J.; Shull, K. R.; Lakrout, H.; Creton, C. *J. Appl. Phys.* **2000**, *88*, 2956.
10. Shull, K.; Flanigan, C.; Crosby, A. *Phys. Rev. Lett.* **2000**, *84*, 3057.
11. Ghatak, A.; Chaudhury, M. K. *Langmuir* **2003**, *19*, 2621.
12. Persson, B. N. J.; Kovalev, A.; Wasem, M.; Gnecco, E.; Gorb, S. N. *Europhys. Lett.* **2010**, *92*, 46001.
13. Mazich, K. A.; Samus, M. A.; Smith, C. A.; Rossi, G. *Macromolecules* **1991**, *24*, 2766.
14. Phanishwar, K; Hakim, M. K.; Ranjan, A. International Conference on Advanced Nanomaterials and Emerging Technologies (ICANMEET), 24–26 July 2013, Chennai, India, **2013**, p 663–665.
15. Krupenkin, T. N.; Fredrickson, G. H. *Macromolecules* **1999**, *32*, 5029.
16. Krupenkin, T. N.; Fredrickson, G. H. *Macromolecules* **1999**, *32*, 5036.
17. Lee, J. -Y.; Cosby, A. J. *Macromolecules* **2005**, *38*, 9711.
18. Baljon, A. R. C.; Robbins, M. O. *Macromolecules* **2001**, *34*, 4200.
19. Tan, H. Z. Y.; McLeish, T. C. B.; Duckett, R. A.; Ward, N. J.; Johnson, A. F.; Donald, A. M.; Butler, M. *Macromolecules* **1998**, *31*, 1348.
20. Weeks, T.; Adolf, D.; McCoy, J. D. *Macromolecules* **1999**, *32*, 1918.
21. Aranson, I. S.; Kalatsky, V. A.; Vinokur, V. M. *Phys. Rev. Lett.* **2000**, *85*, 118.
22. Buxton, G. A.; ; Balazs, A. C. *Macromolecules* **2005**, *38*, 488.
23. Skrzeszewska, P. J.; Sprakel, J.; Wolf, F. A.; de, Fokkink, R.; Stuart, M. A. C.; van der Gucht, J. *Macromolecules* **2010**, *43*, 3542.
24. Tanaka, Y.; Kuwabara, R.; Yang-Ho, N.; Kurokawa, T.; Gong, J. P.; Osada, Y. *J. Phys. Chem. B* **2005**, *109*, 11559.

25. Patil, S.; Ranjan, A.; Sharma, A. *Macromolecules* **2012**, *45*, 2066.
26. Das, S.; Ghatak, A. *J. Mater. Sci.* **2011**, *46*, 2895.
27. Persson, B.; Brener, E. *Phys. Rev. E* **2005**, *71*, 036123.
28. Rubinstein, M.; Colby, R. H. Polymer Physics; Oxford University Press: London, **2003**.
29. Das, A. L.; Mukherjee, R.; Katiyer, V.; Kulkarni, M.; Ghatak, A.; Sharma, A. *Adv. Mater.* **2007**, *19*, 1943.
30. Li, D.; Huang, J.; Kaner, R. B. *Acc. Chem. Res.* **2009**, *42*, 135.
31. Cao, Y.; Andreatta, A.; Heeger, A. J.; Smith, P. *Polymer* **1989**, *30*, 2305.
32. Heinrich, M.; Gruber, P.; Orso, S.; Handge, U. A.; Spolenak, R. *Nano Letters* **2006**, *6*, 2026.
33. Rukhlya, E. G.; Litmanovich, E. A.; Dolinnyi, A. I.; Yarisheva, L. M.; Volynskii, A. L.; Bakeev, N. F. *Macromolecules* **2011**, *44*, 5262.